Path Planning For Robotic Polishing of Sheet Metal Parts

Yuezhi (Sean) Liu (seanliuap@gmail.com)
Ryerson University Faculty of Engineering and Architectural Science
Fengfeng (Jeff) Xi
Ryerson University Faculty of Engineering and Architectural Science
Reza Faieghi
Ryerson University Faculty of Engineering and Architectural Science

Research Article

Keywords: Polishing, Sheet Metal Parts, force planning, deformation, shell element

Posted Date: July 6th, 2021

DOI: https://doi.org/10.21203/rs.3.rs-651044/v1

Path Planning for Robotic Polishing of Sheet Metal Parts

Yuezhi (Sean) Liu[1,a], Fengfeng (Jeff) Xi[1], Reza Faieghi[1]

[1]Department of Aerospace Engineering, Ryerson University, Toronto, Canada

[a]seanliuap@gmail.com

Keywords: Polishing, Sheet Metal Parts, force planning, deformation, shell element

Abstract. Unlike solid parts, the deformation caused by a contact force during robotic polishing of sheet metal parts has become an issue. In this paper, a path planning method is purposed to resolve this issue. This method includes three steps. The first step is to apply the Hertz theory to compute the contact areas between the tool head and the free-form surface of a sheet metal part. The second step is to apply the finite element method to compute the deformation under a contact force. The third step is to reconstruct the deformed free-form surface and modify the contact areas accordingly. The underlying problem is dynamic because the deformed surface shape changes as the tool head moves along a tool path. Based on the proposed method, an optimal path can be determined to achieve full coverage of the entire surface without over or under polishing.

1. Introduction

Sheet metal parts with high-quality surface finish receive a great deal of attention from manufacturing industries. Polishing techniques are usually used to improve the quality of the surface finish on sheet metal parts; nonetheless, the traditional polishing method is time-consuming, costly, and prone to human error. As such, the use of robotic polishing is desired to decrease cost and improve time efficacy. However, robotic polishing of geometrically complex sheet metal parts continues to remain a formidable challenge that impedes the wider implementation of this technology.

One solution that might be able to address the above challenge is to account for the variation of the contact areas between the tool head and the part surface. The size of the contact area between the tool head and the part surface depends on the curvature of a surface under a constant load. As such, for complex geometry, the contact area is expected to change considerably throughout the part, and this leads to under-or over-polish patches in the surface finish, and thus reduced polishing quality [1-5].

Numerous strategies have been proposed to design a robotic path planning method that accounts for the variation of contact areas. A group of proposed methods intends to design a tool path that maximizes the coverage [6-8]. In this context, one approach is to design a tool path according to the size of the contact area [8]. This method works well on curved surfaces with simple geometry, however, it often leads to irregular and computationally expensive tool paths for geometrically complex shapes. Another group of methods involves planning the applied load [9-13]. One popular method for this is to use constant pressure throughout the entire polishing path [9]. However, such methods are also limited to curved surfaces with simple geometry, and cannot compensate for large variations on surface curvatures.

Furthermore, for sheet metal parts, the overall shape can deform under the applied load from the tool head, which is referred to as structural deformation. This will change the curvature of the surface, and in turn, alters the size of the contact area between the tool head and the part surface, making it more difficult to achieve high-quality polishing results. As such, many existing studies in robotic polishing have focused on thick solids or assuming no structural deformation occurs in the part [1-13], and there remains a gap in the knowledge on robotic polishing for sheet metal parts.

In light of the above discussion, the present study introduces a new robotic polishing path planning method that can account for contact area variations of complex surfaces on deformable sheet metal parts. To this end, first, the tool-part contact area is calculated by applying the Hertz theory in combination with the theory of differential geometry for complex surfaces (Section 3.1). Then, the structural deformation of the contact area as a result of the applied force is calculated using the finite element method (FEM) in Section 3.2. Additionally, a method for designing a flexible tool path that is suitable for complex part surface geometry is introduced in Section 4 as a supplementary for this method. Finally, a path planning algorithm is introduced in

Section 5 which makes use of the predicted contact areas and structural deformations to address robotic polishing of sheet metal parts with complex geometry.

2. Problem Statement

The polishing process is an abrasive machining process that requires the polishing tool to press and rub against the part surface. The tool head is attached to the end effector of a robotic arm, and the part surface is fixed in position, as shown in Fig 1.

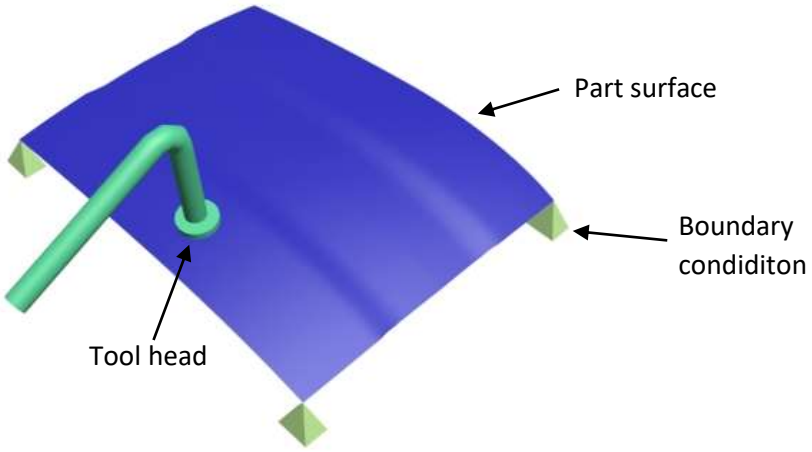

Figure 1. Robotic polishing of a sheet metal part

As the tool head presses against the part surface, a contact area forms between them. To achieve high-quality polishing results, it is crucial to know how the size of the contact area between the tool head and the part surface varies. According to the Hertz theory [14], the contact area between two contacting bodies of solid forms an ellipse. For a curved part surface, the axes of the contact ellipse s are a function of the radii of the surface R, R' at a contact location, and the applied force F.

$$s = f(R, R', F) \tag{1}$$

where s is either the semi-major or semi-minor axis of the ellipse. The radii of the part surface, however, changes as the sheet metal undergoes structural deformation in response to an applied force, which in turn alters the size of the contact area. To determine the true contact area, the change in the radii of the part surface needs to be determined by analyzing its structural deformation. The new radii value can be then used to modify the result calculated from the Hertz theory. If the true contact area needs to be modified for quality purposes, the applied force is adjusted, and the process repeats until the desired size of the contact area is achieved.

This process can be rather tedious. To simplify it, the modification factor (M factor) is introduced in this paper derived from the structural deformation analysis.

$$M_s = \frac{s_{true}}{s_{\text{original}}} \tag{2}$$

The M factor modifies the axes of the contact ellipse calculated using the original local radii to account for the effect of the structural deformation. With this, the true contact area can be directly related to the applied force without the need for any iteration process. The flow chart that reflects this is shown in Fig. 2.

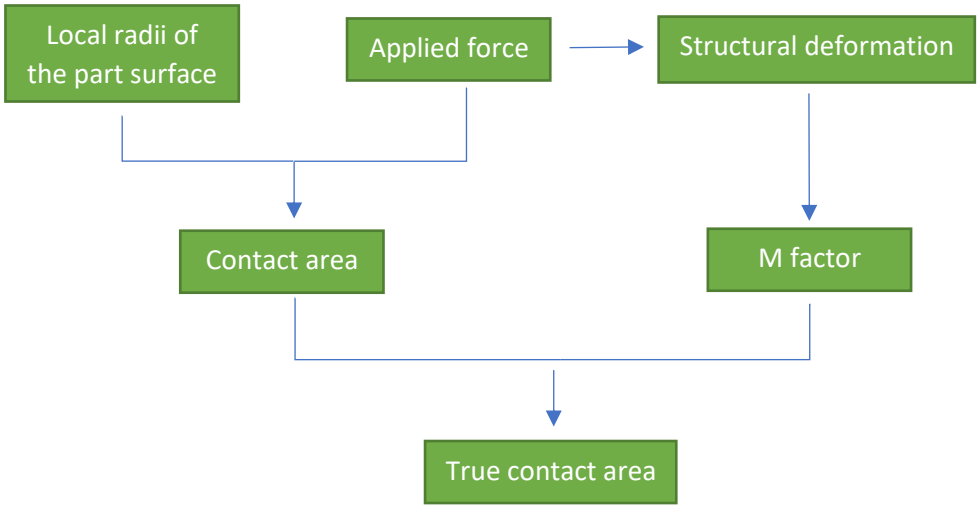

Figure 2. Flow chart of the contact area calculation process using modification factor (instant surface).

3. Basic Theory

3.1 Hertz Theory

When two bodies are in contact, the maximum stress is located at the initial contact point, i.e. the center of the contact area, and can be related to the semi-minor axis b of the ellipse as

$$P_0 = \frac{b}{E(k')\Delta} \tag{3}$$

where $E(k') = \int_0^{\frac{\pi}{2}} \sqrt{1 - k'^2 \sin^2\theta}\, d\theta$ is a complete elliptic integral of the second kind, $\Delta = \frac{1}{A+B}\left(\frac{1-\nu_1^2}{E_1} + \frac{1-\nu_2^2}{E_2}\right)$, $k = \frac{b}{a}$, $k' = \sqrt{1-k^2}$. a semi-major axis. E_i is Young's modulus of the contacting bodies and ν_i are their Poisson ratio, with subscript 1 referring to the tool head, and subscript 2 referring to the sheet metal part. A and B are functions of geometrical properties,

$$A = \frac{1}{4}\left(\frac{1}{R_1} + \frac{1}{R_2} + \frac{1}{R_{1'}} + \frac{1}{R_{2'}}\right) - \frac{1}{4}\sqrt{\left(\left(\frac{1}{R_1} - \frac{1}{R_{1'}}\right) + \left(\frac{1}{R_2} - \frac{1}{R_{2'}}\right)\right)^2 - 4\left(\frac{1}{R_1} - \frac{1}{R_{1'}}\right)\left(\frac{1}{R_2} - \frac{1}{R_{2'}}\right)\sin^2\phi}$$

$$B = \frac{1}{4}\left(\frac{1}{R_1} + \frac{1}{R_2} + \frac{1}{R_{1'}} + \frac{1}{R_{2'}}\right) + \frac{1}{4}\sqrt{\left(\left(\frac{1}{R_1} - \frac{1}{R_{1'}}\right) + \left(\frac{1}{R_2} - \frac{1}{R_{2'}}\right)\right)^2 - 4\left(\frac{1}{R_1} - \frac{1}{R_{1'}}\right)\left(\frac{1}{R_2} - \frac{1}{R_{2'}}\right)\sin^2\phi} \tag{4}$$

where R_i denotes the principal radii of the two contacting bodies, ϕ is the angle between the principal directions of the contacting bodies, and k can be determined by solving the equation below numerically

$$\frac{B}{A} = \frac{\frac{1}{k^2}E(k') - K(k')}{K(k') - E(k')} \tag{5}$$

where $K(k')$ is a complete elliptic integral of the first kind, and $E(k')$ is a complete elliptic integral of the second kind The stress distribution follows

$$P(x', y') = P_0 \left(1 - \left(\frac{x'}{a}\right)^2 - \left(\frac{y'}{b}\right)^2\right)^{1/2} \tag{6}$$

In Eq (4), (x', y') is the coordinate about the origin at the point of initial contact. The applied force is given by

$$F = \frac{2\pi E^2(k')\Delta^2 P_0^3}{3k} = \frac{2\pi b^3}{3kE(k')\Delta} \tag{7}$$

The values of the semi-major axis of the contact area a can be determined with

$$a = \sqrt[3]{\frac{3E(k')}{2\pi k^2}(F\Delta)} \tag{8}$$

To determine the semi-major or semi-minor axis of the contact area with Eq (3) or Eq (8), the material and geometrical properties of the contacting bodies are needed. Lastly, using Eq (3), (6), and (8), a relation between the applied force and the pressure can be derived.

$$P = \left(\frac{3kF}{2\pi\Delta^2 E^2(k')}\right)^{\frac{1}{3}} \left(1 - \left(\frac{x'}{a}\right)^2 - \left(\frac{y'}{b}\right)^2\right)^{1/2} \tag{9}$$

It's easy to see that once the material of the tool and the part surface and the shape of the tool head is chosen, the applied force or the pressure is a function of the principal radii of the surface at a contact location and the applied force. In actual application, the applied force is a control variable, and the principal radii of the surface need to be calculated.

Before the principal radii can be calculated, it requires that the geometry of the part surface be represented with a continuous surface function. This can be achieved by scanning the actual object or converting a CAD model of the part surface into a point cloud. The point cloud data can then be used to curve fit the function [15-17]. In the discussion of the following sections, it is assumed that the part surface is orientated in such a way that the resulting function is represented as a function of x and y coordinates, $f(x, y)$.

For a sheet metal part described by a surface function $f(x, y)$, the principal radii can be calculated with the following steps. First, the two principal directions, namely $D_1 = \left.\frac{dy}{dx}\right|_1 (P)$ and $D_2 = \left.\frac{dy}{dx}\right|_2 (P)$, at a point P on the surface need to be calculated using the theory of differential geometry

[18]. For most surface points, one of the D_is would have a value $D_i < 1$, and the other with $D_i > 1$. Next, two curves need to be generated so that each of the two tangent vectors is pointed towards a principal direction when projected onto the $x - y$ plane. Once these two curves are established, the principal curvatures can be readily determined. The simplest curves to generate are the straight lines when projected onto the $x - y$ plane following along with the principal directions. They are $y_1 = D_1 x + c_1$, and $y_2 = D_2 x + c_2$, and the corresponding curves on the surface can be expressed as and the corresponding curves on the surface can be expressed as

$$\vec{C}_1(x) = \left(x, y_1(x), f\left(x, y_1(u)\right)\right), \quad \vec{C}_2(x) = \left(x, y_2(x), f\left(x, y_2(x)\right)\right) \tag{10}$$

where $\vec{C}_1(x)$ and $\vec{C}_2(x)$ are the curves needed for calculating the principal curvatures, and $\kappa_1(x)$ and $\kappa_2(x)$ are the two curvatures calculated using the theory of differential geometry, based on which the principal radii are

$$R_i(x) = \frac{1}{\kappa_i(x)} \tag{11}$$

For clarity, it is convenient to define the major principal radii to be the greater one of the two, and the minor principal radii as the smaller one. With this, once the material of the part surface and tool head is determined, the semi-axes of the contact ellipse are functions of the contact location and the applied force, $a(x, y, F)$, and $b(x, y, F) = ka$.

For most robotic polishing, the tool usually has a flat surface aside from some special cases that require the tool to be either semi-spherical or cylindrical. For a flat surface, both major and minor principal radii are infinite. With this A and B take the form of

$$A = \frac{1}{2R'} \quad B = \frac{1}{2R} \tag{12}$$

Recall the definition of elliptical integrals, together with the Eq (10), it is required for $R' \geq R$ so that $k \leq 1$. Therefore, R' need to be fixed to the major principal radius, and R to be the minor principal radius. In addition to the value of the major and semi-axis of the ellipse, their orientation also affects the contact area.

3.2 FEM

In the above description, it is assumed that there is no overall structure deformation, which is the case as shown in Fig. 3(a), only with local contact deformation. However, if the surface is simply the shape of a thin shell, the global structural deformation will occur as shown in Fig. 3(b), and the total deformation will be a combination of the cases shown in Fig. 3(a) and Fig. 3(b).

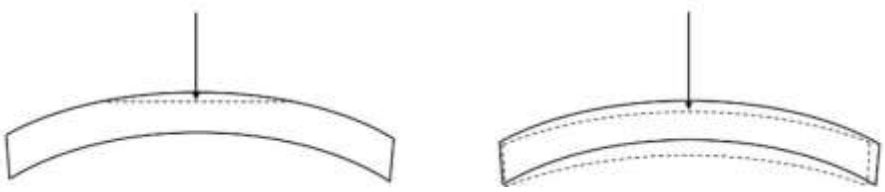

(a) (b)

Figure 3. Deformation of the part surface, with (a) local contact deformation, (b) global structural deformation

For pure structure deformation, which is shown in Fig 3(b), can be calculated using FEM, such as ANSYS, shell181 element for single-layer. The sheet metal is fixed on four corners as shown in Fig. 1. To apply the load in the FEM setting, every element that intersects with the contact area is applied pressure along the surface normal downwards. The pressure value is calculated using Eq (7) based on the position of the center of the element with its relation to the center of the tool head. The results are shown in Fig. 4.

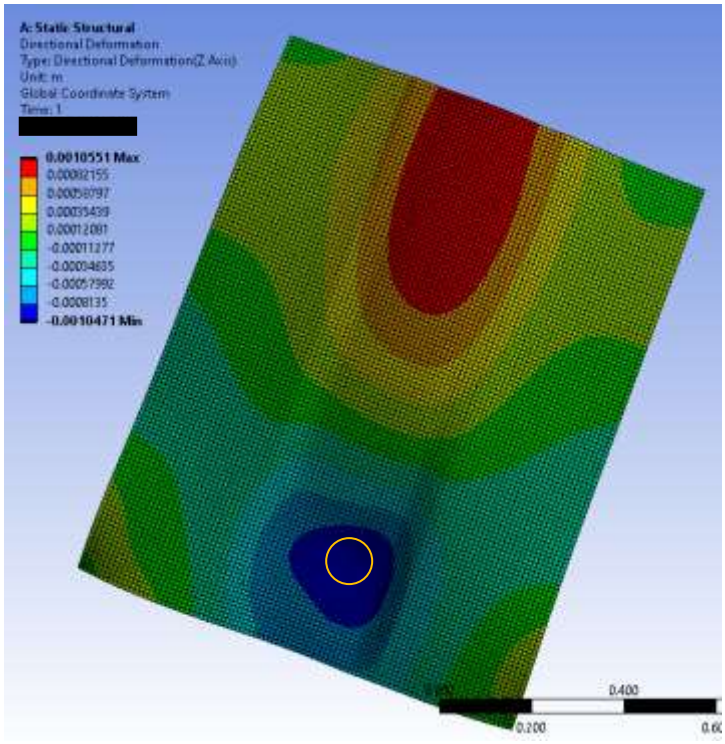

Figure 4. Structural deformation of the sheet metal under the applied force of 200 N, the yellow circle marks the location of the tool head.

The structural deformation changes the geometry of the part surface. Therefore, the contact area between the tool head and the part surface is changed. To update the surface function, the displacement of every node is collected. If the original nodal position is (x_i, y_i, z_i), and displacement vector of every node is (dx_i, dy_i, dz_i), the modification function $df(x, y)$ to the original surface function can be fitted with data set $(x_i + dx_i, y_i + dy_i, dz_i)$. The new surface function will be

$$f_{new}(x, y) = f(x, y) + df(x, y) \tag{12}$$

The reason that the modification function $df(x, y)$ is used instead of directly fitting the new surface using $(x_i + dx_i, y_i + dy_i, z_i + dz_i)$ is that the displacement field (dx_i, dy_i, dz_i) is

smoother than the actual surface in general. Therefore $df(x, y)$ can be fitted using a much simpler polynomial function, which speeds up the process. Moreover, the overall displacement is usually much smaller than the geometrical feature of the surface. Depends on the function used for fitting, it may not be able to pick up the small changes in the shape, if $f_{new}(x, y)$ is fitted using $(x_i + dx_i, y_i + dy_i, z_i + dz_i)$. The data set $(x_i + dx_i, y_i + dy_i, dz_i)$ is plotted in Fig. 5 for illustration. The new surface functions can be then used to calculate the true contact area.

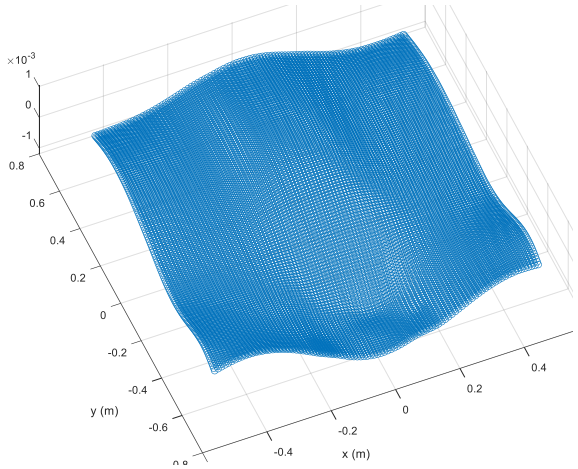

Figure 5. plot of displacement using the result from FEM

4 Path Design

It starts with designating waypoints that represent the overall shape of the path. The path is straight lines that go through waypoints and are smoothly connected by a circular arc as shown in the figure below, where the blue line is the path and red dots are waypoints. Waypoints 1 and 2, 3 and 4, 5 and 6, and so on are connected with straight lines, and waypoints 2 and 3, 4 and 5, 6 and 7, and so on are connected with circular arcs, as shown in Fig. 6.

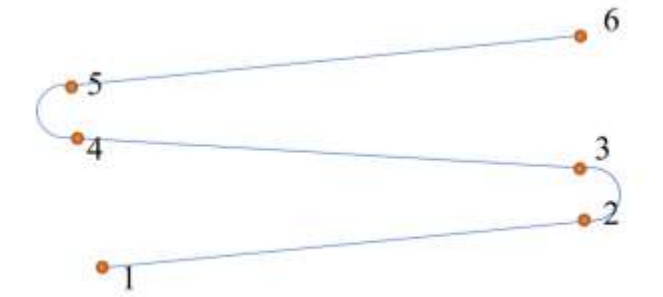

Figure 6. Tool path generation

The reason a circular arc was used to connect the straight lines is that whenever there is a sharp turning on the path, it requires deceleration before the turn and acceleration afterward. This does not only lower the efficiency of the overall process but also in some cases reduce the quality. Next, starts with the path planning in 2D. For a straight-line pass from $P_1 = (x_1, y_1)$ to $P_2 = (x_2, y_2)$, it can be expressed with the equation

$$y = kx + a \ , \quad k = \frac{y_2 - x_1}{y_2 - x_1} \ , \quad a = -\frac{y_1 x_2 + x_1 y_2}{y_2 - x_1} \tag{14}$$

For two straight lines, one goes from $P_1 = (x_1, y_1)$ to $P_2 = (x_2, y_2)$ with $y_1 = k_1 x + a_1$, the other goes from $P_3 = (x_3, y_3)$ to $P_4 = (x_4, y_4)$ with $y_2 = k_2 x + a_2$, there can be a circle to which they both tangent to. The circular arc goes from P_2 to P_3 can be determined as follow. First, the line that perpendicular to y_1 and pass-through P_2 can be expressed with

$$y_{1\perp} = -\frac{1}{k_1} x + a_{1\perp} \ , \quad a_{1\perp} = \frac{y_2^2 - y_1 y_2 + x_1 x_2 - x_2^2}{y_2 - y_1} \tag{15}$$

The same can be done for the line that is perpendicular to y_2 and passing through P_3 for $y_{2\perp}$. While the circular center of this arc is the intersection of $y_{1\perp}$ and $y_{2\perp}$, this requires precise placement of P_2 and P_3 so that the arc can smoothly connect both straight lines. This is unreasonable to achieve during the planning of the waypoints. Instead, when the equations that represent both lines y_1 and y_2 will intersect, unless parallel, their intersection point is

$$P_I = (x_I, y_I) = \left(\frac{a_2 k_1 - a_1 k_2}{k_1 - k_2}, \frac{a_1 - a_2}{k_1 - k_2}\right) \tag{16}$$

From this point, we can derive a line that bisects the angle between y_1 and y_2, which is

$$y_b = k_b x + a_b \ , \quad a_b = y_I - k_b x_I$$

$$k_b = \tan\left(\frac{1}{2}(atan_2(y_2 - y_1, x_2 - x_1) + atan_2(y_3 - y_4, x_3 - x_4))\right) \tag{17}$$

If y_1 and y_2 are parallel, they do not intersect. However, in term of programming the path, to avoid writing extra lines of code, simply let $x_1 = x_1 + e$, or $y_1 = y_1 + e$, or do the similar for any other points whenever the circumstance arises, where e is a small number that is well under the error of tolerance. The same can be done for the cases when $x_1 = x_2$ or $y_1 = y_2$. The circular center of this arc is the intersection of $y_{1\perp}$ and y_b, which is

$$P_c = (x_c, y_c) = \left(\frac{a_b + a_{1\perp} k_1 k_b}{k_1 k_b + 1}, \frac{(a_b - a_{1\perp}) k_1}{k_1 k_b + 1}\right) \tag{18}$$

The radius is the distance from P_c to P_2, $r = |P_c - P_2|$. Now, the equation for the line that perpendicular to y_2 and pass-through P_c can be derived.

$$y_{2\perp} = -\frac{1}{k_2} x + a_{2\perp} \ , \quad a_{2\perp} = \frac{y_c(y_3 - y_4) + x_c(x_3 - x_4)}{y_3 - y_4} \tag{19}$$

To achieve a smooth transition from the arc to the straight line, P_3 is replaced with the intersection of $y_{2\perp}$ and y_2

$$P_3' = \left(\frac{a_{2\perp}+a_2k_2^2}{k_2^2+1}, \frac{(a_2-a_{2\perp})k_1}{k_2^2+1}\right) \tag{20}$$

The expression for the arc is

$$C_{arc}(t) = (r\cos t + x_c, r\sin t + y_c) \tag{21}$$

Solve for $C_{arc}(t_i) = P_2$, and $C_{arc}(t_f) = P_3$ to find the range of t. Note that just because the arc goes from P_2 to P_3, it doesn't mean that t move from t_i to t_f. Depends on the overall orientation of the lines t can move from t_i to t_f or t_f to t_i.

Once the 2D case is planned out, for the 3D case, if the surface is expressed with $S = (x, y, z(x, y))$, the 2D curve can be projected onto the surface with

$$C = \left(x, y(x), z\big(x, y(x)\big)\right) \quad \text{or} \quad C = \left(x(t), y(t), z\big(x(t), y(t)\big)\right) \tag{22}$$

To determine the exact coordinate location of the tool head at each input update, the following equation can be solved numerically.

$$L = \int_{t_i}^{t_{i+1}} \left|\big(x'(t), y'(t), z'(t)\big)\right| \, dt \quad \text{or} \quad L = \int_{x_i}^{x_{i+1}} \left|\Big(1, y'(x), z'\big(x, y(x)\big)\Big)\right| dx \tag{23}$$

where L is the distance moved at each input update from the last. The tangent vector can be calculated with.

$$\vec{T}(x) = \frac{\big(1, y'(x), z'(x, y(x))\big)}{\left|\big(1, y'(x), z'(x, y(x))\big)\right|} \quad \text{or} \quad \vec{T}(t) = \frac{\big(x'(t), y'(t), z'(t)\big)}{|(x'(t), y'(t), z'(t))|} \tag{24}$$

To have the tangent vector always point toward the direction that the tool head is moving, we adopt the arc length parameter. From Eq(23), while solving for x_i, L is expressed as a function of x or t as

$$L = \int_a^x \left|\Big(1, y'(u), z'\big(u, y(u)\big)\Big)\right| du \quad \text{or} \quad L = \int_a^t \left|\big(x'(u), y'(u), z'(u)\big)\right| du \tag{25}$$

The incremental direction of L points toward the direction of the motion of the tool head. Let l be a parameter, so

$$x(l) = x(L(x) = l) \quad \text{or} \quad t(l) = t(L(t) = l) \tag{24}$$

With this, $\vec{T}(l)$ will always point toward the direction of the motion of the tool head. The normal vector can be calculated with.

$$\vec{n}(x, y) = \pm \frac{\vec{s}_x \times \vec{s}_y}{|\vec{s}_x \times \vec{s}_y|} \tag{25}$$

The $\pm$ is assigned according to the orientation of the surface normal to ensure that the normal points toward the tool head, not away.

5. Deformation-Based Path Planning

It is convenient to plan the path along or approximately along with one of the principal directions. Doing so, the step-over distance can be planned as one of the axes of the contact area ellipse. To ensure the polishing track is even, one of the axes of the contact ellipse should be constant throughout the path. To conduct path planning, the principal directions of the part surface are examined at waypoints as shown in Fig. 7. By following the principal directions, and using the path design method described above, a raster path with a circular arc step-over connection is generated on the sheet metal part given in Fig. 1.

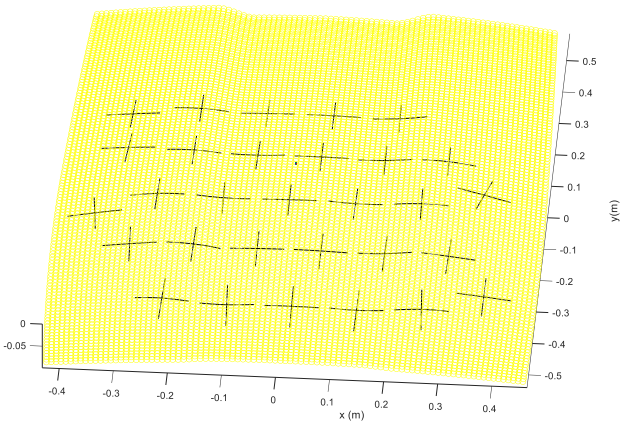

Figure 7. The plot of the principal directions.

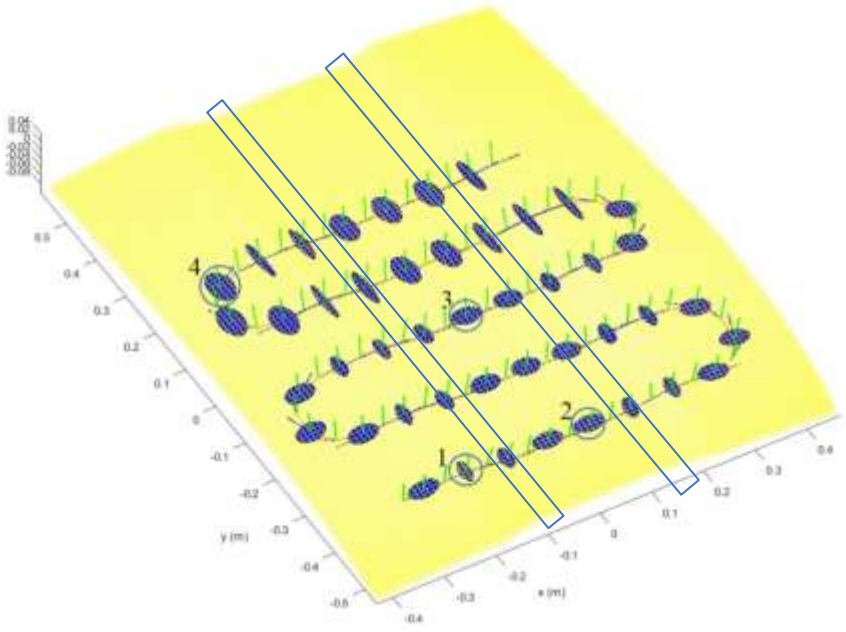

Figure 8. The plot of the contact areas along a tool path on the sheet metal without deformation

In Fig. 8, the red line represents the path, the blue lines represent the direction of tangent vectors at the waypoints, the green lines represent the direction of normal vectors, and the blue disks are the contact areas. The material for the surface is chosen to be Aluminum alloy with Young's module and Poisson's ratio being 71GPa and 0.32, respectively. The material for the tool head is chosen to be hard rubber with Young's module, and Poisson's ratio being 100MPa and 0.49. For this simulation, the effect of the structural deformation is not considered. The tool used in the simulation is a flat disk with a radius of 7cm, and a constant 200N is applied by the tool head along the path. The step-over distance is set according to the size of the tool. The four circles mark the tool locations, which are used for structural deformation analysis in the next section.

The two blue stripes indicate the area of the surface where it is concave. Strictly speaking, the contact areas calculated using Eq (3) and (8) would be the contact area formed from the tool pushing up from the underside of the surface. Polishing on a concave surface is when the force is applied from a direction to which the part surface is perceived as concave, and similarly, polishing on a convex surface is when the force is applied from a direction to which the part surface is perceived as convex. Normally, to polish a concave area, the tool head needs to be semi-spherical or cylindrical, of which its radii are less than the local radii of the concave area. However, for simplicity and illustration purpose, the contact areas near those two stripes are not treated differently and are plotted as if the surface is convex.

Fig. 8 shows that the contact area varies according to the curvature of the surface. Using Eq (3) or (8), the applied load can be properly adjusted to compensate for the difference in the size of the contact areas. In addition to that, the orientation of the contact ellipse changes according to the principal direction. It also illustrates that the semi-major axis and semi-minor axis of the contact ellipse exchange depending on which principal radius is larger.

By analyzing the structural deformation of the four locations marked in Fig. 8 using FEM, its effect on the axis of the contact ellipse is determined. The results are list in Table 1.

F=200 N	Without Structural Deformation		With Structural Deformation	
	Semi-major (mm)	Semi-minor (mm)	Semi-major (mm)	Semi-minor (mm)
Location 1	21.6	10.9	22.1	11.2
Location 2	28.2	15.1	29.3	15.6
Location 3	26.4	19.3	27.9	20.1
Location 4	38.5	21.6	41.7	22.4

Table 1. List of semi-axes under the conditions of with and without Structural Deformation with applied force being 200 N.

The M factor from Eq (2) can be calculated using the data in Table. 1 as the ratio of the semi-axis of the contact ellipsis between with and without the structural deformation.

$$M_s = \frac{s_{with}}{s_{without}} \tag{28}$$

To properly plan a path that can achieve full coverage of the polishing surface without over-polishing, the knowledge of the size of the contact area along the entire path is needed. Although the contact area without the structural deformation is easy to calculate, it can be very tedious to calculate the structural deformation at every possible contact location on the part surface. However, a good approximation can be derived by examining the M factor at a few selected locations under a few different applied force values. Using that information, it is possible to fit a three-variable polynormal function M_s as a function of principal radius, proximity to the location boundary conditions, and the loading force.

$$M_s(r,p,F) = \sum a_{ijk}\, r^i p^j F^k \tag{29}$$

where the principal radius is the radius along that step-over direction. Proximity can be defined as the sum of the inverse distance square from the tool location to the corners,

$$p = \sum (d_i + C)^{-2} \tag{30}$$

where C is a constant and is chosen to be 0.01 here. Note that different boundary conditions will need different proximity functions. If the part surface is fixed in position on all edges, the proximity can be defined as the sum of the inverse distance square from the tool location to the edges. In general, the structural deformation results in larger contact areas. Additionally, the results in Table 1. also illustrate that the modification to the contact areas due to the structural deformation varies depending on the radii of the part surface at the location where the contact occurs, as well as the proximity of the said location to the areas where the boundary conditions are applied.

To better understand the relationship between M factor and the variable that determines it, an example geometry is generated to study the effect of the structural deformation on contact areas. The geometry is illustrated in Fig. 9

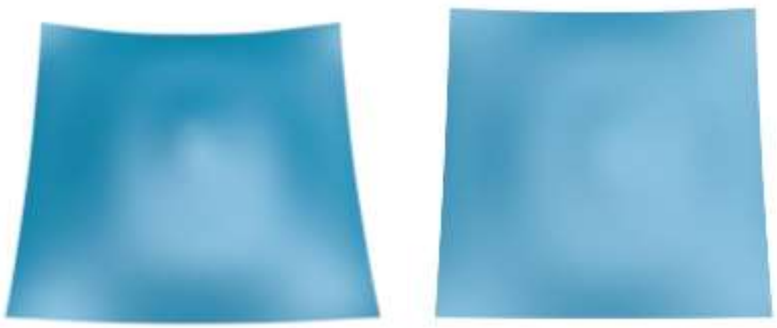

(a) (b)

Figure 9 Sample geometries with (a) being surface 1, and (b) surface 2.

In Fig. 9, surface 1 and surface 2 have similar geometrical features, only surface 2 is flatter than surface 1.

M Factor on Convex Surface

To examine the M factor on the convex surface, four locations on both surfaces are chosen and their contact areas are plotted in Fig 10. The force is applied from a direction to which the part surface is perceived as convex.

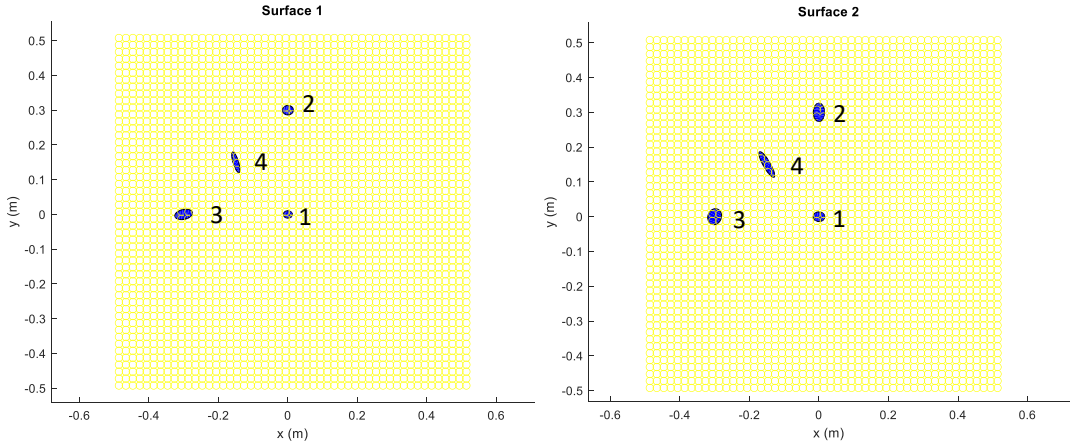

(a) (b)

Figure 10. Plot of contact areas on convex surfaces with applied force being 100 N

The relationship between the M factor at those aforementioned locations and the applied force is plotted in Fig. 11 (a) and (b). Along with the relationship between the M factor the applied force for the sheet metal in Fig. 9 that is plotted in Fig. 11(c), it shows that the deformation is approximately in a linear relationship with the applied force.

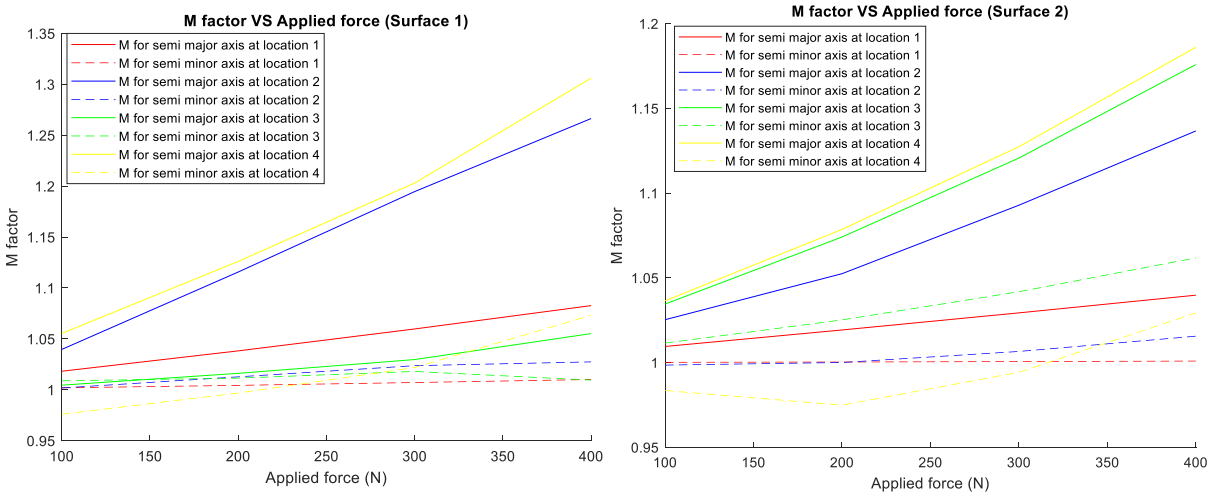

(a) (b)

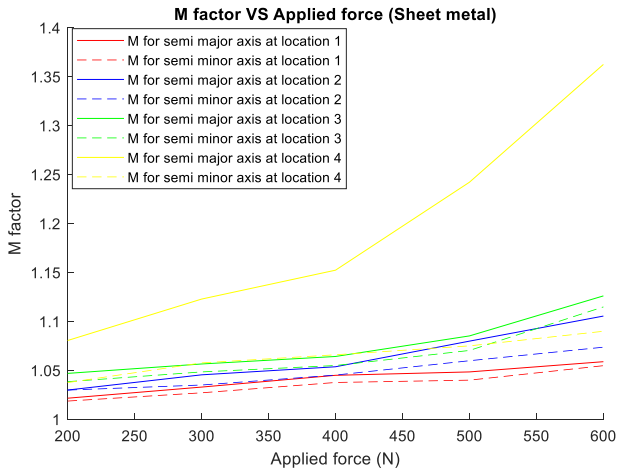

(c)

Figure 11. The plot of the M factor vs the applied force for convex surfaces.

In Fig. 11 (a) and (b), the M factor at location 4 for semi-minor axis for both surface 1 and 2 is less than 1 when the applied force is less than 250 N. This indicates that the accuracy of the M factor for the semi-minor axis at that location is less than what would be desirable. The reason for that is the ellipse at that location for both surfaces has very high eccentricity. This can have several effects. First, high eccentricity results in a narrow ellipse. If the semi-minor axis is comparable with the size of the element used in FEM, the applied pressure assigned in the FEM procedure can not properly describe the pressure distribution of Eq (9), which results in the error in displacement calculation. The average length and width of the element used in the FEM for this study is 0.01m, which is not much smaller than the semi-minor axis of the contact ellipse at location 8. Secondly, a high eccentricity of the contact area is resulted from the part surface has a much higher curvature in one principal direction than the other at that location. This can cause instability in the fitting of the polynormal function used to describe the original surface and the surface displacements depend on the fitting methods. Because The calculation of the M factor relies on FEM and fitting, which both are approximation methods, extra precaution is needed during the initial planning. Especially, it is necessary to avoid choosing the direction of the semi-minor axis as the step-over direction when ellipses with high eccentricity are present.

M Factor on Concave Surface

To examine the M factor on the concave surface, the same four locations on both surfaces are used and their contact areas are plotted in Fig 12. The force is applied from a direction to which the part surface is perceived as concave. To calculate the contact area, the tool is chosen to be spherical with a curvature radius of 0.2m for surface 1, and 0.4m for surface 2. The radius of the tools is taken as a negative value for Eq (4).

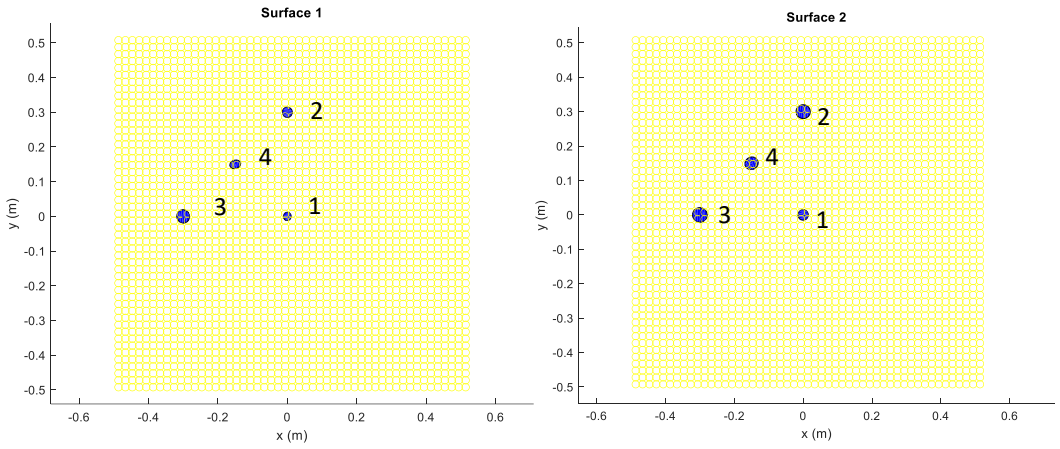

(a) (b)

Figure 12 Plot of contact areas on concave surfaces with applied force being 100 N

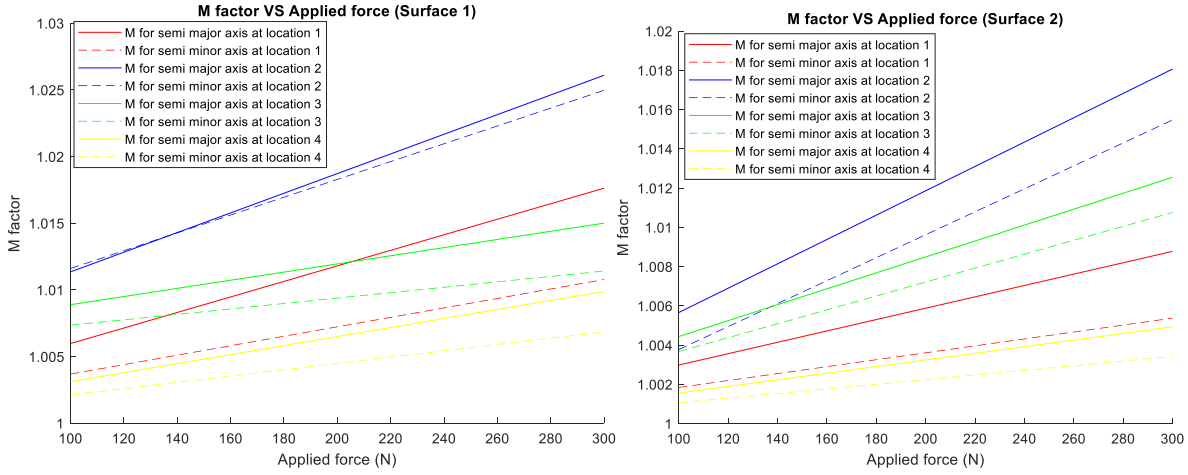

(a) (b)

Figure 13. The plot of the M factor vs the applied force for concave surfaces.

Fig. 12 shows that the contact areas on the concave surfaces are much more circular than those on the convex surface. Additionally. Fig. 13 shows that the values of the M factor remain very close to one. This indicates that when polishing the concave surfaces, the effect on the structural deformation on the contact areas is very small, and can therefore be ignored.

Accuracy and the Rate of Convergency

The accuracy of the function $M_s(r,p,F)$ depends on the number of sample locations of which the deformation is analyzed using FEM. Due to the nearly linear relationship between the M factor and the applied force, the highest order of the F^k from Eq (29) can be capped at no more than 2. Four sample locations and two different loading forces at each location are a good start. With these eight data points, a polynomial of pseudo-degree of one can be fitted

$$M_s(r,p,F) = a_{000} + a_{100}r + a_{010}p + a_{001}F + a_{110}rp + a_{011}pF + a_{101}rF + a_{111}rpF \quad (31)$$

Pseudo-degree of n is defined as the highest order of a variable. To check the accuracy, additional two sample locations are chosen to calculate the M factor resulted from the FEM analysis. The results are then compared with the calculated value from Eq (29). If the accuracy is not satisfactory, the new data from those two sample locations are combined with the previous data, and together to fit a new function of $M_s(r, p, F)$. The pseudo degree of $M_s(r, p, F)$ can be increased gradually as needed with the highest order of the F being capped at two. This process repeats until the satisfied accuracy is achieved, and then the form of the function M_s is obtained.

To check the rate of convergence of the above method, The M factor for surfaces 1 and 2 are fitted using the data from the first four locations shown in Fig. 11, at applied force being 100N and 300N. Four additional locations shown in Fig. 14 are chosen, at which the M factor is calculated using the data from FEM, and is compared with the values calculated from the fitted equation. The results are listed in Tab. 2 and 3.

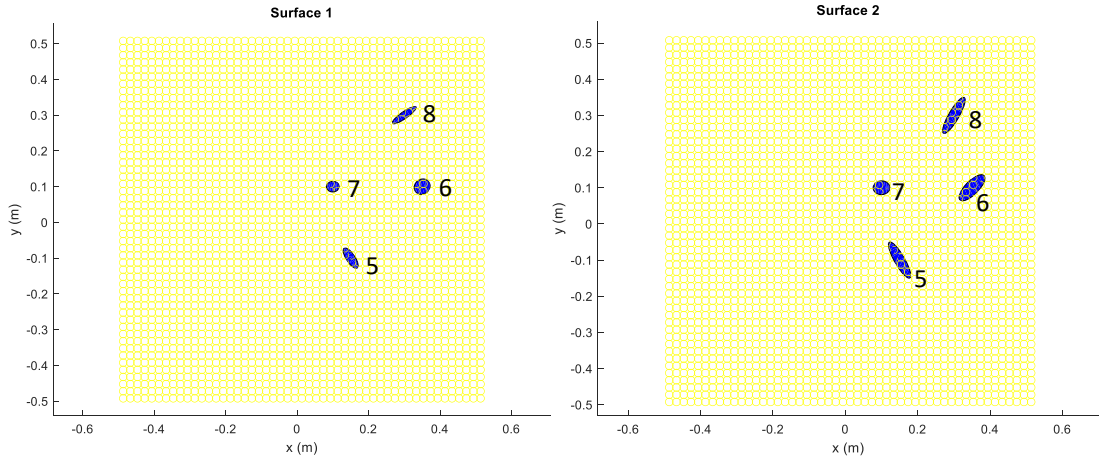

Figure 14. Plot of contact areas on convex surfaces with applied force being 250 N

Surface 1	M factor (with FEM)		M factor (fitted equation)		Difference %	
F=250 N	Semi-major	Semi-minor	Semi-major	Semi-minor	Semi-major	Semi-minor
Location 5	1.196	1.042	1.252	1.083	4.7	3.9
Location 6	1.083	1.061	1.092	1.033	0.8	2.6
Location 7	1.017	0.979	1.009	1.130	0.8	15.4
Location 8	1.246	1.135	2.388	0.852	91.7	25.0

Table 2. Comparison of the value M factor with the equation of the M factor being fitted with the data at 4 locations for surface 1

Surface 2	M factor (with FEM)		M factor (fitted equation)		Difference %	
F=250 N	Semi-major	Semi-minor	Semi-major	Semi-minor	Semi-major	Semi-minor
Location 5	1.243	0.994	1.477	1.018	18.8	2.4
Location 6	1.074	1.049	1.105	1.144	2.9	9.1
Location 7	1.021	1.013	1.034	1.002	1.3	1.1
Location 8	1.247	0.989	1.810	0.924	45.1	6.6

Table 3. Comparison of the value M factor with the equation of the M factor being fitted with the data at 4 locations for surface 2

Tab. 2 and 3 show that there is not much difference in accuracy when this method is applied to the surface with different flatness. Additionally, the accuracy of the fitted M factor is low for the location where the contact ellipse has high eccentricity. For next iteration, the data of the location 5 and 6 at applied force being 100N and 300N are included to fit the new M factor, and the values of the M factor function is compared with the value of the M factor from FEM. The results are listed in Tab. 4 and 5 and show a moderate improvement of accuracy.

Surface 1	**M factor (with FEM)**		**M factor (fitted equation)**		**Difference %**	
F=250 N	Semi-major	Semi-minor	Semi-major	Semi-minor	Semi-major	Semi-minor
Location 7	1.017	0.979	1.041	1.003	2.4	2.5
Location 8	1.246	1.135	1.615	1.052	29.6	7.3

Table 4. Comparison of the value M factor with the equation of the M factor being fitted with the data at 6 locations for surface 1

Surface 2	**M factor (with FEM)**		**M factor (fitted equation)**		**Difference %**	
F=250 N	Semi-major	Semi-minor	Semi-major	Semi-minor	Semi-major	Semi-minor
Location 7	1.021	1.013	1.015	1.034	1.0	2.1
Location 8	1.247	0.989	1.385	0.957	10.8	3.2

Table 5. Comparison of the value M factor with the equation of the M factor being fitted with the data at 6 locations for surface 1

The above procedure is repeated for the sheet metal. The 8 locations are shown in Fig. 15, and the results are listed in Tab. 6 and 7.

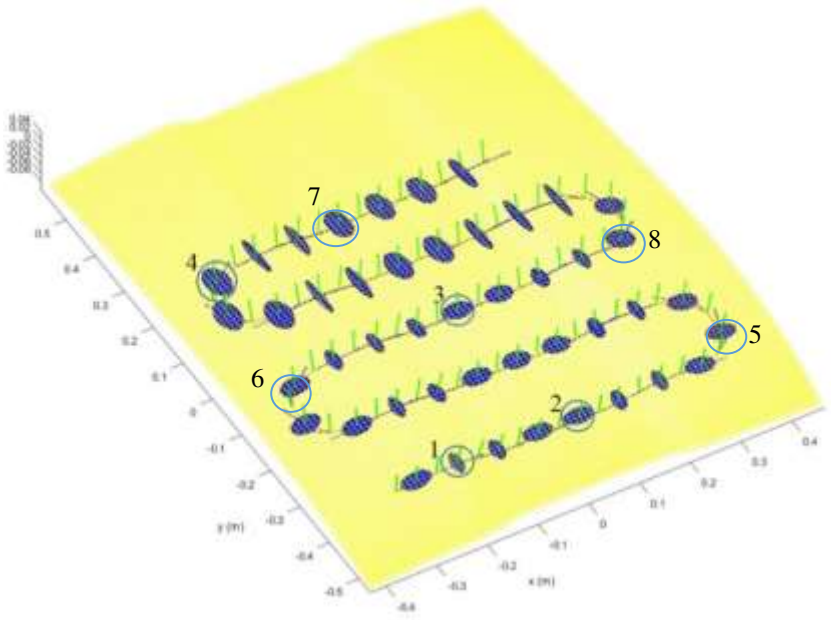

Figure 15. The plot of the contact areas along a tool path on the sheet metal without deformation

Sheet metal F=400 N	M factor (with FEM)		M factor (fitted equation)		Difference %	
	Semi-major	Semi-minor	Semi-major	Semi-minor	Semi-major	Semi-minor
Location 5	1.074	1.051	1.136	1.026	5.8	2.4
Location 6	1.148	1.064	1.132	1.032	1.4	3.0
Location 7	1.193	1.082	1.281	1.121	7.4	3.6
Location 8	1.134	1.058	1.064	1.049	6.2	0.7

Table 6. Comparison of the value M factor with the equation of the M factor being fitted with the data at locations from 1 to 4 for the sheet metal in Fig. 15

Sheet metal F=400 N	M factor (with FEM)		M factor (fitted equation)		Difference %	
	Semi-major	Semi-minor	Semi-major	Semi-minor	Semi-major	Semi-minor
Location 7	1.193	1.082	1.151	1.093	3.5	1.0
Location 8	1.134	1.058	1.146	1.067	1.1	0.9

Table 7. Comparison of the value M factor with the equation of the M factor being fitted with the data at locations from 1 to 6 for the sheet metal in Fig. 15

Tab. 6 and 7 shows that the same procedure yield better accuracy overall for the sheet metal. This is because the geometry of the sheet metal is simpler than the sample geometry of surfaces 1 and 2. In addition, the sheet metal has a strict symmetry along the middle line. As the result, for a more complex surface, it would require the data from more contact locations obtained through FEM to fit the M factor with desirable accuracy.

Since both r and p are functions of x, y, ultimately M_s can be expressed as a function of x, y, i.e. the contact location on the part surface. However, it would not be wise to fit the M_s as a function x, y using the coordinates of the contact location. This is because that while there are some underlying relationships between the M factor and the r and p, there is no identifiable relationship between the M factor and the x, y coordinates. The true axes of the contact ellipse can be related to the applied force and the contact location with

$$a_{true} = M_a(x, y, F) \cdot a(x, y, F) \quad \text{and} \quad b_{true} = M_b(x, y, F) \cdot k(x, y) \cdot a(x, y, F) \qquad (32)$$

With this, the raster path in Fig. 8 is adjusted, and the applied force is modified to ensure an even polishing track. The result of this is illustrated in Fig. 16.

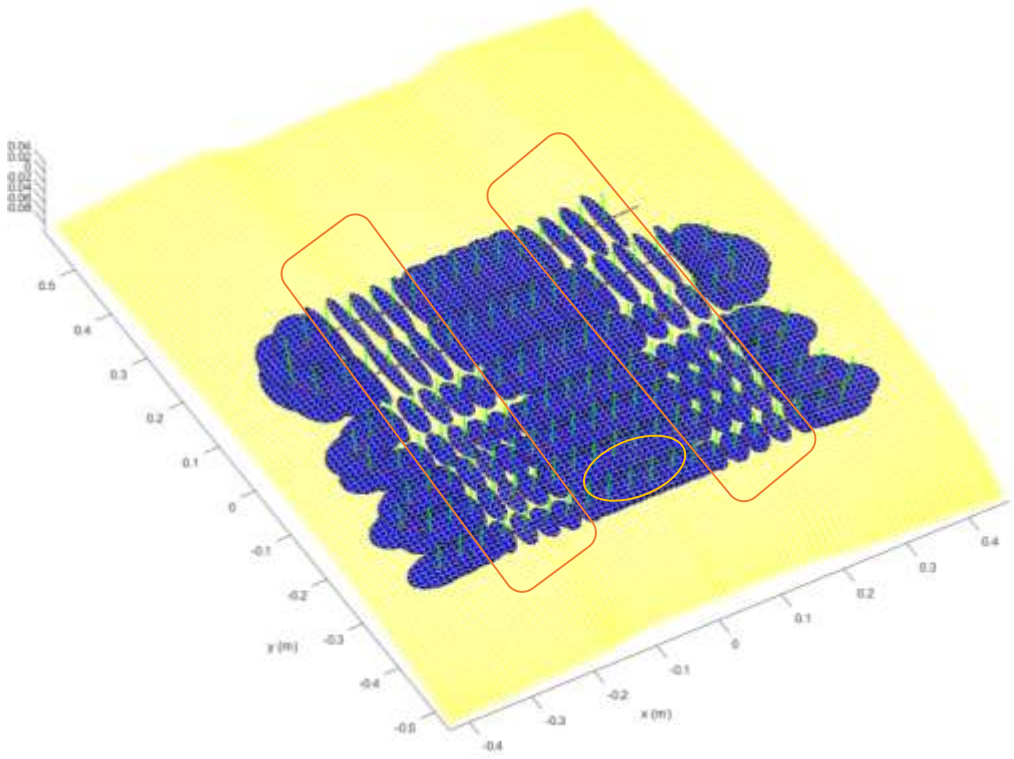

Figure 16. The plot of the even polishing track along a tool path

In Fig. 16, the applied force is set at 500 N gradually reducing to 200 N with the step-over distance being adjusted accordingly. The applied force at certain locations, marked by the yellow circle as an example, is increased individually to match the width of the contact area with the neighboring ones. Note that if the modified contact area is used to calculate the structural deformation with FEM, the deformation results will change, and this in turn will once again change the contact area. For some ultra-high precision applications, a repeated iteration procedure needs to be carried out to obtain a highly accurate result. Importantly, it is necessary to assume that the overall deformation of the sheet metal is small and within the linear elastic limit. It should be only used on applications when the material of the sheet metal is linear elastic and applied force is small that will not cause nonlinear deformation.

Interpolation Relation

The waypoints illustrated in Fig. 17 are sample points. The waypoints for the polishing robot to follow are far denser. For efficiency, it is not necessary to determine all the precise input force values at every waypoint, but rather an interpolation relation can be derived from two sequential sample points. For a flat tool,

$$\Delta \propto \frac{R'R}{R'+R} \tag{33}$$

If the sample points are close enough or the part surface is flat enough, the principal radii of the part surface, as well as the M factor, varies approximately linearly. If b_t is kept constant, b would

be inversely linear. Additionally, it can be assumed from Eq (5) that if the change in the principal radii is small, k can be considered as varying approximately linearly, and this, in turn, results in $E(k')$ varies linearly. With this, from Eq (7),

$$F \propto \frac{1}{kE(k')}\left(\frac{1}{M_b}\right)^3 \frac{R'+R}{R'R} \tag{34}$$

where k, $E(k')$, M_b, R', R, are all linear functions between two sequential sample points and their value can be determined using a simple linear interpolation for any waypoint. The force value can then be calculated straightforwardly for any waypoints in between the sample points. In terms of the choice for the sample points, if the area of a part surface is relatively flat or uniform, they can be chosen sparsely for that area. If there is a sharp change in the area of a part surface, the sample points need to be more densely packed. The yellow squares in Fig. 11 mark the area where more sample points may need to be chosen. Nevertheless, the overall complexity of the planning using this method can be reduced or increased based on the accuracy requirement of an application.

6. Conclusion

In this paper, a method for the planning for robotic polishing of sheet metal parts is purposed. This method consists of several components. First, a method that can precisely calculate the contact areas between the tool hand and a complex curved surface using Hertz's theory and the theory of differential geometry is introduced. With this, the difference in the size of the contact area due to the surface geometry can be compensated by adjusting the applied force accordingly. Next, to compensate for the changing in size of the contact area due to the structural deformation, the structural deformation using FEM. Lastly, the data as the result of the structural deformation analysis is used to fit the contact area modification function, which can be used to estimate the change in contact area due to the structural deformation throughout the entire sheet metal surface. The analysis of the sample geometry in the paper shows that the modification to the contact area due to the structural deformation is negligible for polishing on the concave surface. It also shows that when polishing on the convex surface, the accuracy of this method reduces at the locations where the contact ellipses have high eccentricity, and it is necessary to avoid choosing the direction of the semi-minor axis as the step-over direction when ellipses with high eccentricity are present. By comparing the accuracy of the fitted M factor function on the sample geometry with the function on the sheet metal, it shows that the fitted M factor function is more accurate on the surface with simple geometry especially when the geometry has a certain symmetry. Lastly, it is worth noting that this method is developed based on the assumption of the deformation being linear elastic, and would not work accurately for any application that requires nonlinear deformation.

Declarations

a. Funding

Natural Science and Engineering Research Council of Canada

b. Conflicts of interest/Competing interests

Not applicable

c. Availability of data and material

Not applicable

d. Code availability

Not applicable

e. Ethics approval

Not applicable

f. Consent to participate

Not applicable

g. Consent for publication

The authors of this paper give consent for publication

h. Authors' contributions

The first author is a PhD student, and the second and third authors are the supervisors.

Reference

[1] L. Zhang, H.Y. Tam, C.-M. Yuan, Y.-P. Chen, Z.-D. Zhou; An investigation of material removal in polishing with fixed abrasives; Proceedings of the I MECH E Part B Journal of Engineering Manufacture 216 (2002) 103–112.

[2] C. J. Julien, J. M. Linares, J. M. Sprauel; Improving tool wear and surface covering in polishing via toolpath optimization; J Mater Process Technol 213(10) (2013)1661–1668.

[3] S. Z. Wang, J. Liu, L.H. Zhang; Dual-rotor tool path generation and removal error analysis in active feed polishing; Appl Opt 52(28) (2013)6948–6955.

[4] Y. W. Sun, D. Y. Feng, D. M. Guo; An adaptive uniform toolpath generation method for the automatic polishing of complex surfaces with adjustable density; Int J Adv Manuf Technol 80(9) (2015)1673–1683.

[5] J. Liu, S. Z. Wang, C. L. Zhang, L. H. Zhang, H. N. Chen; Path planning and parameter optimization of uniform removal in active feed polishing; Opt Eng 54(6) (2015)065101.

[6] H. Y. Tam, O. C. H. Lui, A. C. K. Mok; Robotic polishing of free form surfaces using scanning paths; J Mater Process Technol 95(1–3) (1999)191–200.

[7] E.S. Topal; The role of step-over ratio in prediction of surface roughness in flat end milling," International Journal of Mechanical Sciences; 51(2009)782–789.

[8] L. Zhang, Y. Han, C. Fan, Y. Tang, X. Song; Polishing path planning for physically uniform overlapof polishing ribbons on freeform surface; Int J Adv Manuf Technol 92(2017) 4525–4541

[9] M. Rososhansky, F. Xi, and Y. Li; Coverage Based Tool Path Planning for Automated Polishing Using Contact Stress Theory; IEEE Int Conf Auto Science and Engineering, 2010

[10] A. Roswella, F. Xi, G. Liu; Modelling and analysis of contact stress for automated polishing; Int J Machine Tools & Manufacture 46 (2006) 424–435

[11] L. Liao, F. Xi, and G. Liu, "Adaptive Control of Pressure Tracking for Polishing Process," ASME J Manuf Sci Eng, to appear in April, 2010.

[12] Jianming Zhan; An improved polishing method by force controllingand its application in aspheric surfaces ballonet polishing; Int J Adv Manuf Technol 68(2013)2253–2260

[13] F. Tian, Z. Li, C. Lv, G. Liu; Polishing pressure investigations of robot automatic polishing on curved surfaces; Int J Adv Manuf Technol; 87(1)(2016)639-646.

[14] A.P. Boresi, R.J. Schmidt, O.M. Sidebottom, Advanced mechanics of materials, Fifth ed., Wiley, 1993.

[15] S. Fleishman, D. Cohen-Or, C. Silva; Robust moving least-squares fitting with sharp features; ACM Trans. Graph. 24 (3) (2005) 544-552

[16] Y. Wang, J. Zheng; Curvature-guided adaptive T -spline surface fitting; Computer-Aided Design 45 (2013) 1095–1107

[17] M. Blane, Z.B. Lei, D.B. Cooper; The 3L Algorithm for Fitting Implicit Polynomial Curves and Surfaces to Data, IEEE Trans. Pattern Analysis and Machine Intelligence, 22 (3)(2000) 298-313

[18] T. Banchoff, S. Lovett; Differential Geometry of Curves and Surfaces; CRC Press, Taylor & Francis Group, LLC, 2010